ELSEVIER

Catalysis Today 69 (2001) 87–93

CATALYSIS TODAY

www.elsevier.com/locate/cattod

The ejector-driven monolith loop reactor — experiments and modeling

Robert R. Broekhuis*, Reinaldo M. Machado, Andrew F. Nordquist

Air Products and Chemicals, Inc., 7201 Hamilton Blvd., Allentown, PA 18195, USA

Abstract

A novel catalytic gas–liquid reactor configuration, consisting of a monolithic reactor with a liquid-motive ejector as gas–liquid distributor is introduced as a retrofit or alternative to an agitated slurry reactor. The ejector distributes gas and liquid to the channels of a monolith reactor at velocities greater than those attainable with gravity-driven flow, intensifying mass transfer and reaction in a compact reactor. Pressure drops measured using this configuration do not conform to models from the literature. A strong effect of liquid coalescence properties was observed. Until fully predictive pressure drop and gas–liquid distribution models become available, successful scale-up will depend on pressure-drop data measured with industrial process conditions and fluids. Current literature models for mass transfer underpredict laboratory autoclave reaction results, indicating a need for further model development, and in the interim requiring pilot-scale testing for scale-up purposes.

Keywords: Gas–liquid reactor; Ejector-driven monolith loop reactor; Two-phase pressure drop; Mass transfer

1. Introduction

Monoliths have been used in gas-phase catalytic applications for many years. They are particularly prevalent in mobile and stationary environmental application areas, including automotive exhaust catalysts. The use of monoliths to catalyze gas–liquid reactions is not as widespread. This area has attracted considerable academic interest for over 10 years, resulting in several literature reviews [1,2]. As a class of gas–liquid reactions, hydrogenations have attracted the most interest, as evidenced by academic literature [3–6] as well as the patent literature [7,8].

Edvinsson and Cybulski [4] compared monoliths against trickle-bed reactors for a selective hydrogenation, and identified conditions under which monoliths hold an advantage. However, most patents for the use of monoliths to conduct hydrogenations are in areas where the traditional technology is a stirred-tank slurry reactor. It is perhaps more pertinent, therefore, to compare the performance of monoliths against slurry reactors. Cybulski et al. [6] perform such a comparison in a modeling analysis. Advantages of monolith reactors over batch stirred-tank slurry reactors include a substantial decrease in catalyst handling, more flexibility in design and scale-up, and the elimination of certain selectivity problems associated with batch slurry reactor operations. Heiszwolf et al. [9] propose a monolith loop reactor in which liquid is circulated through the monolith reactor by means of a pump-around loop, using traditional liquid distribution devices, such as spray nozzles. Gas is introduced into the reactor by gravity-driven natural circulation. A batch hydrogenation is conducted by continuously circulating liquid through the monolith until conversion is complete; the conversion per pass is typically small. Heiszwolf et al.

* Corresponding author.

0920-5861/01/$ – see front matter
PII: S0920-5861(01)00358-3

Nomenclature

a	specific interfacial area (m^2/m^3)
Ca	capillary number, $\eta_L v/\sigma$ (–)
d_b	bubble diameter (m)
d_c	internal monolith channel dimension (m)
D	diffusion coefficient for gaseous species (m^2/s)
f_L	friction factor for liquid-only flow (–)
f_{LG}	friction factor for gas–liquid flow (–)
g	gravitational acceleration (m/s^2)
k_{GLS}	overall composite mass transfer coefficient, based on total geometric area (m/s)
k_{ij}	mass transfer coefficient between phases i and j (m/s)
L	monolith channel length (m)
L_j	slug length for phase j (m)
P	pressure (Pa)
Re_L	Reynolds number relative to liquid phase, $\rho_L(u_L + u_G)d_c/\eta_L$ (−)
Sc	Schmidt number, $\eta_L/\rho_L D$(−)
u_i	superficial velocity of phase i (m/s)
v	channel velocity, $u_L + u_G$ (m/s)
Greek characters	
δ	film thickness (m)
ε_i	volume fraction of phase i (–)
η_L	liquid-phase viscosity ($N\,s/m^2$)
ρ_L	liquid-phase density (kg/m^3)
σ	surface tension (N/m)

[9,10] propose models for the pressure drop and mass transfer associated with the gas–liquid flow through monolith reactors. The gravity-driven flow of gas and liquid is effective for small reactor diameters, but gas–liquid distribution may be less uniform for larger reactors.

A novel reactor technology being developed at Air Products and Chemicals combines the concept of a monolith loop reactor with gas–liquid ejector technology, in which the ejector replaces the traditional liquid distribution device. The liquid-motive ejector entrains and compresses recycled hydrogen gas. When properly engineered, the ejector also serves as an excellent gas–liquid contactor, presaturating the liquid before it enters the reactor, and produces a fine dispersion of gas bubbles in liquid, which results in excellent gas–liquid distribution to the monolith. Because the ejector serves as a gas compressor, the gas–liquid dispersion can be delivered to the inlet of the reactor at a pressure greater than the outlet pressure. Compared to a gravity-driven monolith reactor, greater superficial velocities through the monolith channels can be attained, resulting in higher rates of mass transfer and reaction. This is particularly valuable for applications requiring monoliths with channel densities greater than 400 channels per square inch (cpsi), which offer greater geometric surface areas for catalysis.

Scale-up of ejector-driven monolith loop reactors requires engineering models for pressure drop and mass transfer. Models proposed in the literature include some based on single-channel measurements and others based on monoliths with traditional distribution devices. It is our goal to measure pressure drops and mass transfer rates in ejector-driven monoliths and ascertain whether the data conform to literature models.

2. Experimental methods

The experimental setup used to conduct our experiments is depicted in Fig. 1. It incorporates a 30-l hold tank, a centrifugal pump delivering flowrates up to 24 l/min at a differential pressure of 0.46 MPa, a gas–liquid ejector sized to match the pump characteristics, and a tube containing a stack of monolithic elements with an inside diameter of 0.05 m and a length of 0.15–0.6 m. Instrumentation includes gas and liquid flowmeters, differential and direct pressure gauges. The liquid temperature is controlled using a water-cooled coil. Monolith stacks were built using 400 or 600 cpsi elements from Corning, each either 0.05 or 0.15 m long. No attempt was made to align channels between adjoining segments, nor was any spacing left between segments. The entire stack was wrapped with expandable PTFE gasket tape to minimize bypassing.

The setup operates at ambient temperature, with the hold tank open to ambient pressure. Various aqueous solutions were used as the liquid phase, and air or nitrogen as the gas phase.

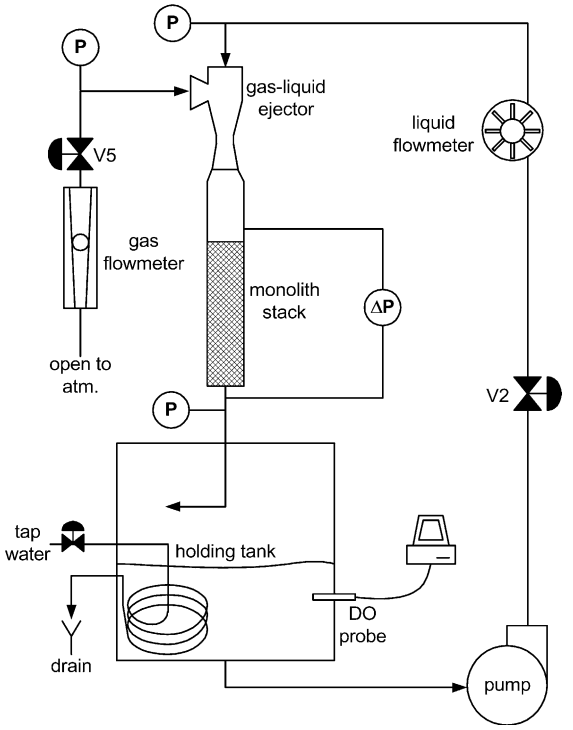

Fig. 1. Schematic of equipment used to determine pressure drops and gas–liquid mass transfer in ejector-driven monoliths.

3. Pressure drop

3.1. Literature review

For a uniform approach to pressure-drop modeling, we will relate all models to the following expression for pressure drop through a channel:

$$\Delta P_{\text{fric}} = 4f\frac{1}{2}\rho_{\text{L}}v^2\frac{L}{d_{\text{c}}} \tag{1}$$

in which $v = u_{\text{L}} + u_{\text{G}}$ is the channel velocity, the sum of liquid and gas superficial velocities. For downflow, the frictional pressure drop is equal to the measured pressure drop plus the static head component

$$\Delta P = \Delta P_{\text{fric}} - \rho_{\text{L}} g L \varepsilon_{\text{L}}, \quad \varepsilon_{\text{L}} = \frac{u_{\text{L}}}{u_{\text{L}} + u_{\text{G}}} \tag{2}$$

The expression for the liquid holdup ε_{L} reflects the common assumption that gas and liquid move through the monolith channels with identical total velocities, i.e. in plug flow. At flow conditions typically seen in high-channel-density monoliths (200 cpsi and up), the flow is laminar: $Re_{\text{L}} < 2000$. Laminar channel flow is described by the Hagen–Poiseuille equation. For round or square channels, this translates to the friction factor

$$f_{\text{L}} = \frac{16}{Re_{\text{L}}} \text{ or } (f\,Re)_{\text{L}} = 16 \tag{3}$$

Deviations from square channel geometry can result in a value of $(fRe)_{\text{L}}$ that deviates from 16. On first approximation the relative deviation for gas–liquid flow should be similar, so that it is convenient to relate gas–liquid pressure-drop results to the liquid-only situation. Eq. (3) should describe the flow of liquid through a monolith channel. For gas–liquid flow, additional assumptions are needed. If we assume that only the liquid phase contributes to pressure drop, the friction factor model reduces to

$$f_{\text{LG}} = f_{\text{L}}\varepsilon_{\text{L}} \text{ or } f_{\text{LG}}Re_{\text{L}} = (f\,Re)_{\text{L}}\varepsilon_{\text{L}} \tag{4}$$

Comparison with actual data shows that this expression consistently underpredicts pressure drops; clearly, the gas phase contributes to pressure drop in some way. Heiszwolf et al. [9] found that they could model their results using a pseudo-homogeneous model

$$f_{\text{LG}}Re_{\text{L}} = \text{constant} \tag{5}$$

This model implies that gas and liquid slugs contribute equally to the pressure drop. For the model to transition smoothly into the single-phase model as liquid holdup increases, the constant $f_{\text{LG}}Re_{\text{L}}$ should be equal to $(fRe)_{\text{L}}$. However, it was found that the value of $f_{\text{LG}}Re_{\text{L}}$ appears to vary with monolith channel density, ranging from 18 for 200 cpsi to 28 for 600 cpsi. Apparently, Eqs. (1) and (5) do not adequately describe the effect of the channel dimension on the pressure drop.

The pressure drop contributed by the gas slugs is attributed either to surface tension effects or to induced flow patterns in the liquid slugs at the liquid–gas boundary. The lack of the surface tension and slug length as model parameters is troubling. The good correspondence between measurements and model is most likely due to the fact that neither slug lengths nor surface tensions varied much in the pressure-drop data set used to construct the models. A model capturing variations in these parameters would be valuable in scaling to reaction systems with different distribution devices, gas–liquid material properties, and

flow characteristics. An entry-region friction model proposed by Heiszwolf et al. [10] includes the slug length L_L as a variable. Using a correlation suggested by entrance-region theory, with adjustable parameters fit to literature data, they arrive at

$$f_{LG}Re_L = (f\,Re)_L \varepsilon_L \left[1 + 0.065\left(\frac{L_L}{d_c Re_L}\right)^{-0.66}\right] \quad (6)$$

In many pressure-drop studies, the liquid slug length is not measured. Because there is no broad data set covering industrial conditions, the equation and its parameters are likely to describe only a subset of conditions that may be encountered in industrial operation.

3.2. Experimental results

Pressure-drop data was collected using a variety of physical configurations (monolith stacking heights, channel densities) and several aqueous liquid phases (deionized water, 0.05, 0.10 mol/l Na_2SO_4). The superficial liquid velocity is determined primarily by the pressure at which liquid is presented to the ejector, and also somewhat by the pressure in the ejector chamber, which is controlled by the gas-throttling valve. The superficial gas velocity is determined by both the gas and the liquid pressures feeding the ejector. The lower the liquid pressure (and, therefore, the liquid flowrate), the lower the gas flowrate. At a given liquid flowrate, the gas flowrate may be manipulated using the gas-throttling valve.

The operating conditions are, therefore, confined to a triangular area on a superficial velocity map — an example is shown in Fig. 2. The maximum superficial gas velocity is achieved with both gas and liquid valves fully open. Two boundary curves extend from the unrestricted superficial velocities. One curve results from throttling the liquid valve, while the gas valve remains fully open; along this curve, both gas and liquid superficial velocities decrease. The other curve results from throttling the gas valve, while leaving the liquid valve open; while the superficial gas velocity decreases along this curve, the superficial liquid velocity increases slightly, due to the decreasing pressure in the ejector chamber.

Fig. 3 shows pressure-drop results for liquid-only flow as a function of liquid velocity for deionized water and 0.10 mol/l Na_2SO_4. The data points fall along the same line, reflecting the fact that the liquid viscosities and densities are very similar. The value of $(fRe)_L$ follows from the slope of the line, and is about 15.5 — very close to the expected value of 16.

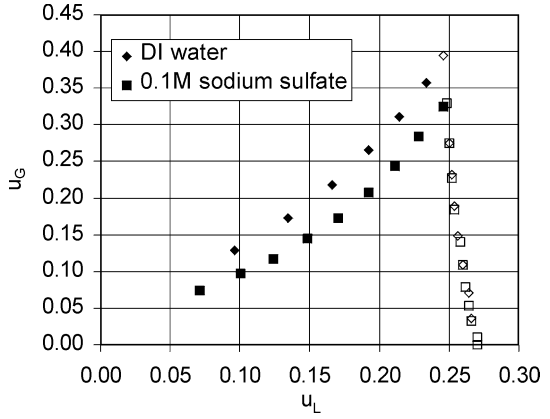

Fig. 2. Superficial velocity map for operation of the ejector in conjunction with a monolith stack consisting of eight 15 cm elements of 600 cpsi cordierite monoliths; results for deionized water and sodium sulfate solution. Open symbols represent the gas-throttled curve and solid symbols the liquid-throttled curve.

Many gas–liquid pressure-drop data were collected. All follow similar trends; for clarity, we will focus on a subset of the collected gas–liquid pressure-drop data, measured using a 1.22 m stack of 600 cpsi monoliths, along the boundary curves of the superficial velocity

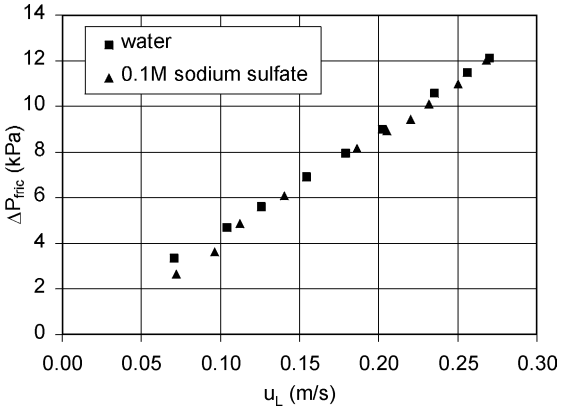

Fig. 3. Pressure-drop data for liquid-only flow through a monolith stack consisting of eight 15 cm elements of 600 cpsi cordierite monoliths; results for deionized water and sodium sulfate solution.

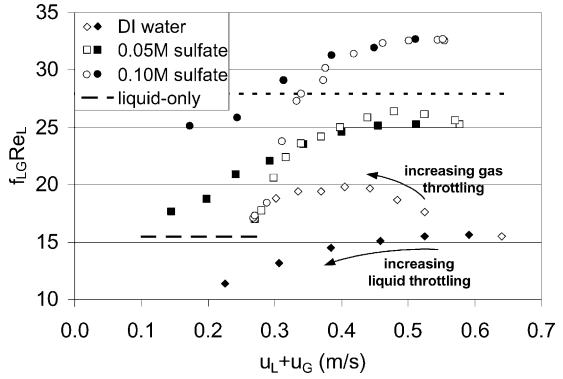

Fig. 4. Pressure-drop results for gas–liquid flow through a monolith stack consisting of eight 15 cm elements of 600 cpsi cordierite monoliths. Open symbols represent the gas-throttled curve; solid symbols the liquid-throttled curve. The dashed line indicates the results for liquid-only experiments and the dotted line the correlation by Heiszwolf et al. [9]: $f_{LG}Re_L = 28$.

map. These data, shown in Fig. 4, demonstrate a large increase of pressure drop with electrolyte concentration. Since the liquid-only results did not vary with ionic strength, this effect must be due to the interactions of the gas phase and the liquid phase. Decreased bubble coalescence in electrolyte solutions [11] usually leads to a smaller steady-state bubble size in turbulent electrolyte solutions, which may result in shorter gas and liquid slug lengths. The entry-region friction model (Eq. (6)) predicts that shorter slugs lead to larger pressure drops, which is consistent with our results.

The open symbols on Fig. 4 represent data measured along the gas-throttled curve of the superficial velocity map for which the gas holdup varies from 0 to around 50%. In the limit of 0% gas holdup, $f_{LG}Re_L$ approaches $(fRe)_L$, shown as the dashed line. The friction factor increases with gas holdup. $f_{LG}Re_L$ reaches a maximum or a plateau with further increases in gas holdup. This suggests that, initially, the introduction of gas into the flow causes additional frictional losses, but that as the volume fraction of gas increases, the friction drops due to the smaller contact area of liquid slug to channel wall.

The solid symbols represent data measured along the liquid-throttled curve. The gas and liquid velocities decrease simultaneously as the liquid flow is throttled, so the gas holdup remains high, between 40 and 60%. For the ionic solutions at high superficial velocities, the $f_{LG}Re_L$ curves coincide with the gas-throttled curves, suggesting that gas holdup does not strongly affect the pressure drop under these conditions. At lower superficial velocities, the curves diverge with higher pressure drops for high-gas-holdup flow than for low-gas-holdup flow. The $f_{LG}Re_L$ curve for DI water lies below the liquid-only results: the effect of extra drag due to the introduction of the gas bubbles is smaller than the reduced drag due to the smaller surface fraction of liquid slugs.

The data presented in Fig. 4 demonstrate that a predictive model for the pressure drop of gas–liquid flow through monoliths must take into account the gas and liquid superficial velocities separately (rather than just the total velocity) and must also account for the effect of the phase distribution. The latter is most properly expressed in terms of a slug length distribution but can probably be captured in terms of an average slug length.

The pseudo-homogeneous model (Eq. (5)) predicts a constant value of $f_{LG}Re_L$, which is clearly not in agreement with Fig. 4. The entry-region friction model (Eq. (6)) is more promising and scientifically more appealing. A problem with any model featuring the slug length as a variable, however, is that slug lengths are rarely measured in full distributor–monolith configurations. Slug lengths characterized in experimental apparatuses do not directly translate to industrial equipment because the phase distribution so strongly depends on the physical means of delivering gas and liquid to the monolith. If we assume that gas slug lengths result from uniformly sized bubbles each entering a single monolith channel, the liquid slug length can be directly calculated from the bubble size

$$L_L = \frac{1-\varepsilon_G}{\varepsilon_G}\frac{\pi}{6}\frac{d_b^3}{d_c^2} \tag{7}$$

Bubble sizes may be estimated by visual observation or using published engineering correlations, and industrial process equipment could be tailored to produce the desired bubble size distribution. Conversely, we can back-calculate the bubble size from experimental data using Eqs. (6) and (7). This calculation, applied to our data, yields bubble sizes of 1.7–2.5 mm for DI water, 1.1–1.5 mm for electrolyte solutions, which seems reasonable.

For scale-up of commercial equipment, a generically applicable Taylor flow model (when it becomes

available) may be combined with a distribution model describing the slug length as a function of operating conditions; alternatively, semi-empirical hybrid models may be developed for particular distributor/monolith combinations. In any case, additional work covering a greater span of distribution approaches and operating conditions is required.

4. Mass transfer

Hydrogen is transferred to the catalyst surface by gas-to-liquid (G–L) and liquid-to-solid (L–S) transfer processes. In the special case of Taylor flow through a monolith, transfer of hydrogen through the thin liquid film surrounding gas bubbles is often considered to be a third, gas-to-solid (G–S), transfer process. Separate models have been proposed for all the three transfer paths. Here, we will demonstrate that current models do not adequately describe overall mass transfer rates attainable in monoliths.

There is a considerable disagreement among literature correlations for G–L mass transfer [12–14], each displaying rather different functional forms and dependences on primary variables. For example, the order in channel velocity v ranges from 0.5 to 1.2; the order in channel width d_c from -0.5 to 0. Because a unified model does not exist, scale-up for specific applications will for the time being require that actual measurements be carried out using the specific equipment and operating conditions of interest. We are in the process of conducting such experiments for the ejector-driven monolith loop reactor and will report on the results in a separate publication.

For L–S mass transfer, Heiszwolf et al. [10] propose an entry-region model analogous to Eq. (6), with parameters fit to various literature data sources.

$$\frac{k_{LS}d_c}{D} = 3.66\left[1 + 0.152\left(\frac{L_L}{d_c Re\, Sc}\right)^{-0.423}\right], \quad a_{LS} = \frac{4\varepsilon_L}{d_c} \tag{8}$$

The G–S mass transfer path of gas through the liquid film can be described using a simple film diffusion model

$$k_{GS}a = \frac{D}{\delta}\frac{4\varepsilon_G}{d_c} \tag{9}$$

where expressions for the film thickness are given as a function of the capillary number by Irandoust and Andersson [15] for a circular channel and by Heiszwolf et al. [10] for the corner of a square channel.

$$\delta_{circ} = 0.18 d_c(1 - e^{-3.08Ca^{0.54}}) \tag{10}$$

$$\delta_{sq} = 0.36 d_c(1 - 0.7\, e^{-2.25Ca^{0.445}}) \tag{11}$$

The effective film thickness follows from integrating the rate of mass transfer along the perimeter of the channel, and for typical monoliths and flow conditions is about 50% greater than δ_{circ}.

It is tempting to combine the three paths of mass transfer as a combination of steps in series and parallel and thus calculate an overall coefficient for mass transfer. Some caution is required with this approach. For example, some of the correlations for gas–liquid mass transfer include the contribution of transfer to the liquid film, which constitutes a partial overlap with the liquid–solid mechanism. Only when the three mass transfer paths are precisely defined to be non-overlapping, and when the measurements used to derive constituent models reflect these definitions, can an overall coefficient be calculated from these constituent models. At present, this level of rigor has not been applied to the definitions of the mass transfer processes.

A minimum value for the overall mass transfer rate can be deduced from catalytic reaction experiments. We conducted a fast nitroaromatic hydrogenation in an autoclave, where liquid and gas were continuously circulated through an internally mounted monolith. These experiments will be more fully discussed in a separate paper, but some overall conclusions are pertinent here. A comparison between experiment and model results is presented in Table 1. The minimum mass transfer coefficient follows from the assumption that the hydrogen concentration at the catalytic surface is negligible; following this reasoning, $k_{GLS}a > 2.5\,s^{-1}$. Throughout the autoclave the liquid is nearly saturated with hydrogen, so that we can ignore the G–L mass transfer resistance; the effective coefficient is then a combination of the G–S and L–S coefficients, at best the sum of the two. Even with favorable estimates for the variables in Eqs. (8) and (9), $k_{GLS}a < 1.7\,s^{-1}$. Clearly, one or both of these correlations underestimate the rate of mass transfer. So again, more

Table 1
Comparison of results from fast-reaction experiment with model mass transfer predictions

Fast-reaction experiment	Mass transfer models
Measured rate, $r_{H_2} = 247\,\text{mol}\,H_2/m^3\,s$	$d_c = 1.09\,mm$
Measured solubility, $c^*_{H_2} = 100 \pm 5\,\text{mol}\,H_2/m^3$	$u_L = u_G = 0.3\,m/s^a$
Surface concentration, $c^s_{H_2} \geq 0\,\text{mol}\,H_2/m^3$	$L_L/d_c = 1.5^a$
$r_{H_2} = k_{GLS}a(c^*_{H_2} - c^s_{H_2})$	$\rho_L = 824\,kg/m^3$
$\rightarrow k_{GLS}a \geq 2.5\,s^{-1}$	
	$\eta_L = 0.33\,mN\,s/m^2$
	$\sigma = 0.018\,N/m$
	$D_{H_2} = 1.7 \times 10^{-8}\,m^2/s$
	Eq. (8): $k_{LS}a = 1.27\,s^{-1}$
	Eq. (9): $k_{GS}a = 0.44\,s^{-1}$
	$k_{GLS}a \leq k_{LS}a + k_{GS}a = 1.7\,s^{-1}$

[a] Denotes estimated values.

work with the specific equipment and process conditions is required for successful scale-up.

5. Conclusions

An ejector-driven monolith loop reactor can be an attractive replacement for or retrofit to a stirred-tank slurry reactor for gas–liquid reactions such as hydrogenations. The ejector effectively distributes gas and liquid to the channels of a monolith reactor and can do so at velocities greater than those attainable with gravity-driven flow. This enables high rates of hydrogen mass transfer, where it matters most — close to the catalytic surface. Benefits include increased reactor productivity, decreased catalyst handling, and a more flexible process.

Pressure drops across an ejector-driven monolith do not follow a pseudo-homogeneous friction model, which means that phase holdup and distribution must be taken into account in modeling. Non-coalescing liquids such as electrolyte solutions exhibit higher pressure drops, due to smaller average bubble size. A predictive pressure-drop model has not been identified. Also, current models for G–S and L–S mass transfer underpredict the high rate of reaction measured in our laboratories. Therefore, successful scale-up will depend on pressure-drop data and overall rate data measured with industrial process conditions and fluids. We will be carrying out pilot plant studies in the near future using a fast demonstration chemistry so that the results will reflect limits of mass transfer as well as kinetics.

References

[1] S. Irandoust, B. Andersson, Catal. Rev. Sci. Eng. 30 (1988) 341–392.
[2] A. Cybulski, J.A. Moulijn, Catal. Rev. Sci. Eng. 36 (1994) 179–270.
[3] V. Hatziantoniou, B. Andersson, N.-H. Schöön, Ind. Eng. Chem. Proc. Des. Dev. 25 (1986) 964–970.
[4] R.K. Edvinsson, A. Cybulski, Chem. Eng. Sci. 49 (1994) 5653–5666.
[5] H.A. Smits, J.A. Moulijn, W.Ch. Glasz, A. Stankiewicz, React. Kinet. Catal. Lett. 60 (1997) 351–356.
[6] A. Cybulski, A. Stankiewicz, R.K. Edvinsson Albers, J.A. Moulijn, Chem. Eng. Sci. 54 (1999) 2351–2358.
[7] E.A. Bengtsson, US Patent 5 063 043 (1990).
[8] R.M. Machado, D.J. Parrillo, R.P. Boehme, R.R. Broekhuis, US Patent 6 005 143 (1999).
[9] J.J. Heiszwolf, L.B. Engelvaart, M.G. van den Eijnden, M.T. Kreutzer, F. Kapteijn, J.A. Moulijn, Chem. Eng. Sci., in press.
[10] J.J. Heiszwolf, L.B. Engelvaart, M.T. Kreutzer, D.J. Parrillo, F. Kapteijn, J.A. Moulijn, Confidential Report to Air Products and Chemicals, Inc., 1999.
[11] R.R. Lesser, S.A. Zieminski, Ind. Eng. Chem. Fundam. 10 (1971) 260–269.
[12] S. Irandoust, B. Andersson, Ind. Eng. Chem. Res. 28 (1989) 1684–1688.
[13] S. Irandoust, S. Ertlé, B. Andersson, Can. J. Chem. Eng. 70 (1992) 115–119.
[14] G. Berčič, A. Pintar, Chem. Eng. Sci. 52 (1997) 3709–3719.
[15] S. Irandoust, B. Andersson, Chem. Eng. Sci. 43 (1988) 1983–1988.